JOURNAL OF MAGNETIC RESONANCE **132,** 88–95 (1998)
ARTICLE NO. MN981357

Composite Pulse Excitation Schemes for MQMAS NMR of Half-Integer Quadrupolar Spins

Laura Marinelli, Ales Medek, and Lucio Frydman[1]

Department of Chemistry, University of Illinois at Chicago, Chicago, Illinois 60607

Received July 28, 1997; revised December 23, 1997

It has been recently shown that 2D multiple-quantum (MQ) spectroscopy in combination with conventional magic-angle spinning can provide high resolution NMR spectra from half-integer quadrupolar nuclei in powdered samples. In an effort to optimize signal-to-noise in this type of experiments, a systematic investigation on the relative efficiencies that single- and two-pulse excitation schemes exhibit toward the generation of MQ coherences was carried out. Numerical simulations on spin-$\frac{3}{2}$ powders revealed that $x-y$ composite pulse excitations with nutation angles $\theta_y \approx 2\,\theta_x$ maximize the excitation of triple-quantum coherences, yielding about 30% larger signals than those available from single-pulse experiments. This behavior was corroborated experimentally, and its origin elucidated with the aid of analytical derivations. Composite pulse schemes also yielded a superior excitation of MQ coherences in the presence of large shielding offsets, although a simple recipe for optimizing such experiments was not apparent.

Key Words: **solid state NMR; quadrupole nuclei; multiple quantum spectroscopy; composite pulses.**

INTRODUCTION

NMR is a well-established tool for analyzing many structural and dynamic problems of polycrystalline solids (*1, 2*). Crucial to the success of these applications are coherent manipulations which allow one to discriminate among signals arising from inequivalent chemical sites despite the anisotropic character of spin interactions. Although this coherent averaging of anisotropies was achieved decades ago for spin-$\frac{1}{2}$ interactions with the introduction of magic-angle spinning (MAS) and multipulse decoupling (*3–5*), such a goal proved more elusive for the important case of higher half-integer spins ($S = \frac{3}{2}, \frac{5}{2}, \frac{7}{2}, \frac{9}{2}$). The solid state NMR spectra of these nuclei are in general dominated by large quadrupolar anisotropies arising from their interactions with the surrounding electric field gradients (*6, 7*). Although these anisotropies can be bypassed to first order by focusing the NMR observation on the central $-\frac{1}{2} \leftrightarrow +\frac{1}{2}$ transition (*8, 9*), the resulting spectra may still lack chemical resolution due to the presence of substantial second-order effects. Rapid sample rotation can be employed toward the partial narrowing of these central transition quadrupolar powder patterns (*10, 11*), but the absence of a single ''magic'' angle capable of removing all second-order effects still leaves spectra thick with overlapping lines from inequivalent sites.

The overcoming of this important resolution limitation was finally achieved thanks to a deeper theoretical understanding of second-order effects in NMR (*12, 13*). These developments lead to two practical techniques, dynamic-angle spinning (DAS) and double rotation (DOR), capable of removing the central transition anisotropies via complex mechanical manipulations based on multiaxial sample rotations (*14, 15*). Recently we demonstrated that an averaging similar to that occurring in DAS can also be achieved using conventional MAS, if this method is combined with certain forms of 2D multiple-quantum (MQ) spectroscopy involving the correlation of $-m \leftrightarrow +m$ coherence orders within the spin manifold (*16*). The resulting 2D MQMAS technique consequently provides a simple approach to high resolution quadrupolar NMR spectroscopy in solids, whose capabilities have already been demonstrated with several practical applications on different nuclei (*17–21*). In view of the potential usefulness of this approach, considerable efforts have also been devoted during the past years to improve the sensitivity and appearance which characterize MQMAS lineshapes (*22–35*). A signal-to-noise (S/N) question that arose early on in these analyses was related to which route should be adopted for achieving a maximum excitation of the odd MQ coherence orders involved in the experiment. One of the assayed approaches, common in liquid crystalline and isotropic NMR work (*36, 37*), proposed the implementation of such MQ coherence pumping via two pulses separated by a free evolution delay; another approach, derived from solid state ^{2}H NMR experiments (*38–42*), proposed achieving this goal by relying on single-pulse radiofrequency (RF) nutations. Although preliminary studies showed that both

[1] To whom correspondence should be addressed: Department of Chemistry (M/C 111), University of Illinois at Chicago, 845 W. Taylor Street, Room 4500, Chicago, IL 60607-7061. Fax: (312) 996-0431. E-mail: lucio@samson.chem.uic.edu.

1090-7807/98 $25.00

methods can afford useful MQMAS NMR data, it quickly became apparent that the latter approach provides spectra with better S/N ratios (*22, 23, 25*), and consequently this single-pulse excitation strategy has been the one adopted in a majority of chemical studies reported to date.

In an effort to provide a more quantitative basis to these qualitative S/N observations, we embarked on a systematic analysis on the performance that a pulse sequence of the form

$$(\tau_1)_x - \Delta - (\tau_2)_\phi \qquad [1]$$

exhibits toward the excitation of triple-quantum coherences of the type usually involved in MQMAS. This search was carried out as a function of initial and final RF pulse widths τ_1 and τ_2, relative irradiation phases ϕ (with x corresponding to $\phi = 0$) and interpulse delays Δ, variations which clearly cover the two possibilities mentioned above. Notably, it was found that neither of the two alternatives considered so far provides the maximum possible excitation of triple-quantum coherences. Instead, calculations revealed that in the presence of moderate shielding effects the optimum excitation efficiency on spin-$\frac{3}{2}$ powders is achieved by a pulse sequence with $\Delta = 0$ and $\phi = \pi/2$, in essence an x–y composite pulse module (*43*). The improvements resulting from these conditions could be experimentally verified as well as justified on the basis of analytical density matrix derivations. These combined experimental/theoretical analyses were also extended to cases involving large chemical shift offsets; for these cases calculations revealed that despite potentially substantial S/N losses, composite pulses can still provide a superior MQ excitation when compared to the more traditional schemes that have been considered so far. The following sections describe the results of these investigations.

EXPERIMENTAL

All spectra reported in this study were recorded in a laboratory-built NMR spectrometer based on a 4.7-T wide-bore Oxford magnet, a Macintosh-controlled Tecmag pulse programmer (Aries), and broadband homodyne hardware. This system is equipped with an LPI-10 ENI amplifier capable of delivering over 1 kW of RF power into suitably tuned loads, and of executing fast RF phase shifting and on/off switching (settling times < 100 ns). MAS was performed at spinning rates $\nu_r \approx 6$–10 kHz, using a standard 5-mm Doty assembly inserted on a laboratory-built doubly tuned variable-angle spinning NMR probehead. RF irradiation fields in the range 100–150 kHz were used in the different experiments, together with a suitable MQMAS phase cycling of the irradiation and demodulation phases for selecting the appropriate coherence transfer pathways. The resulting data were processed offline using the RMN software (courtesy of Professor P. Grandinetti, Ohio State University); spin calculations were carried out on a SGI work station using specially written C programs. All the investigated samples were purchased from Aldrich and used as supplied except for a cobaltoporphyrin complex, which was synthesized in our laboratory as described elsewhere (*44*).

RESULTS

MQ Excitation in the Absence of Shielding Offsets

As mentioned above, MQMAS is designed to provide high resolution quadrupolar NMR spectra via the 2D correlation of multiple- and single-quantum coherence evolutions. Most experiments of this kind have so far entailed the excitation of triple-quantum coherences, as this process is feasible for all half-integer quadrupole nuclei and the resulting MQ states are usually the easiest to generate. Consequently, we focused our calculations on determining the optimized conditions under which a pulse sequence like that in Eq. [1] will maximize such off-diagonal elements starting from a reduced equilibrium density matrix

$$\rho_{\mathrm{eq}} = a \cdot S_z, \qquad [2]$$

where $a = h\nu/2kT$ represents the high-temperature Boltzmann factor. As has been shown elsewhere (*22, 45*), valuable insight into this excitation process can be obtained by representing its spin Hamiltonian by the simplified rotating frame interaction

$$\mathcal{H}(t) = \begin{cases} \nu_{\mathrm{q}}(\theta, \varphi)[3S_z^2 - S(S+1)] + \nu_{\mathrm{RF}} S_x, & 0 \le t < \tau_1 \\ \nu_{\mathrm{q}}(\theta, \varphi)[3S_z^2 - S(S+1)], & \tau_1 \le t < \tau_1 + \Delta \\ \nu_{\mathrm{q}}(\theta, \varphi)[3S_z^2 - S(S+1)] + \nu_{\mathrm{RF}} S_\phi, & \tau_1 + \Delta \le t < \tau_1 + \Delta + \tau_2 \end{cases} . \qquad [3]$$

The first term in these expressions represents the first-order quadrupole frequency

$$\nu_{\mathrm{q}}(\theta, \varphi) = \frac{(e^2qQ/h)}{4S(2S-1)} \left[\frac{3\cos^2\theta - 1 + \eta \sin^2\theta \cos 2\varphi}{2} \right] \qquad [4]$$

given by a coupling constant e^2qQ/h, an asymmetry parameter η, and angles (θ, φ) defining the relative orientation of the external field B_0 with respect to the quadrupolar tensor. The second term in $\mathcal{H}(t)$, acting only during the duration of the RF pulses, represents the nutations introduced by these fields as given by their strength ν_{RF} and the spin operators defining

their orientations. Equation [3] neglects a number of potentially important factors such as the time dependence introduced on $\nu_q(\theta, \varphi)$ by the sample spinning, or the effects introduced by shielding and second-order quadrupole offsets. The first of these approximations will be justified by the short intervals that the pulse sequences end up having when compared with typical rotor period durations; details about the effects of the offsets are further discussed in the following paragraph.

Given the excitation Hamiltonian in Eq. [3], the MQ generation process can be quantified by propagating the initial density matrix according to

$$\rho(\tau_1, \Delta, \tau_2) = e^{-iH(t)\tau_2}\, e^{-iH(t)\Delta}\, e^{-iH(t)\tau_1}\, \rho_{eq}\, e^{iH(t)\tau_1}\, e^{iH(t)\Delta}\, e^{iH(t)\tau_2} \quad [5]$$

and then considering the fate of the ρ_{14}, ρ_{41} off-diagonal elements defining the $-\frac{3}{2} \leftrightarrow +\frac{3}{2}$ spin coherences. A numerical procedure capable of implementing such propagation over powdered samples was written, and allowed to search for the optimized (τ_1, Δ, τ_2) durations and relative phase shifts ϕ that will maximize these elements for a series of experimentally relevant $(e^2qQ/h)/\nu_{RF}$ ratios. These five-dimensional numeric searches consistently revealed that excitation sequences involving $\Delta = 0$, $\phi = \pi/2$ will yield the largest triple-quantum coherences. Figure 1 shows a series of bidimensional renderings of these searches meant to illustrate the effects that the resulting sequence will have on the triple-quantum excitation as a function of the three remaining parameters: $\theta_1 = \nu_{RF}\,\tau_1$, $\theta_2 = \nu_{RF}\,\tau_2$ and $(e^2qQ/h)/\nu_{RF}$. Although the positions of the absolute maxima in these plots are slightly dependent on this latter ratio an efficient MQ excitation can be observed over a range of conditions in the neighborhood of $\theta_1 = 0.4$ cycles, $\theta_2 = 0.8$ cycles. These are consequently good starting parameters upon attempting the study of an unknown sample, susceptible to optimizations according to the calculations by adjusting both pulse widths while preserving a $\tau_2/\tau_1 \approx 2$ ratio. Notice that in addition to these absolute maxima the MQ calculations predict alternative local maxima, including two located in the single-pulse nutation curves ($\tau_1 = 0$ or $\tau_2 = 0$), which correspond to those that were described in earlier MQMAS optimizations studies (*22, 25, 26*). For all $(e^2qQ/h)/\nu_{RF}$ ratios the numerical simulations reveal that the intensities of MQ elements at these local maxima are about 30% smaller than those available upon using optimized $x-y$ composite pulses, implying that traditional single-pulse approaches require almost 70% longer acquisition times than these newer composite pulse counterparts to achieve spectra with comparable S/N ratios.

The predictions of these numerical calculations were

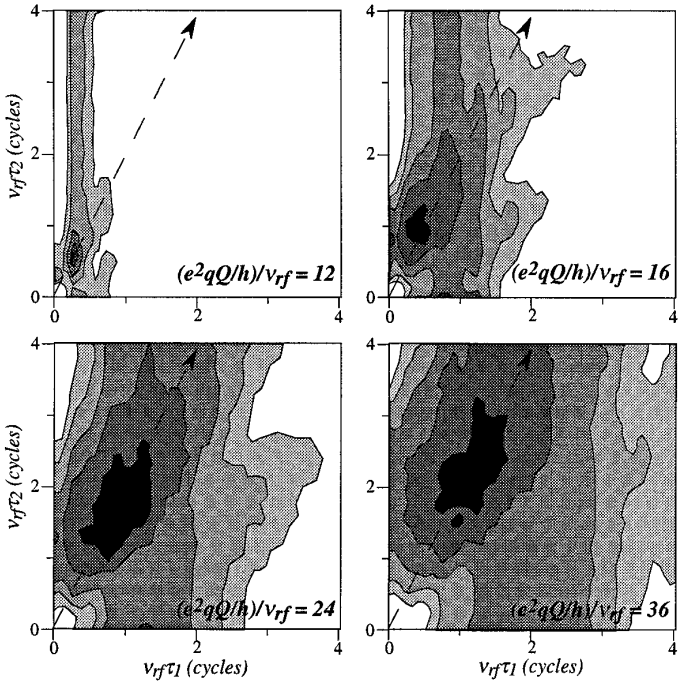

FIG. 1. Triple-quantum excitation profiles (magnitude), describing the application of $x-y$ composite pulses on a spin-$\frac{3}{2}$ powder as a function of nutation pulse lengths and of different $(e^2qQ/h)/\nu_{RF}$ ratios. Calculations result from propagating the Hamiltonian in Eq. [3] ($\Delta = 0$, $\eta = 0$, $\nu_{RF} =$ 100 kHz) for over 100 crystallite orientations using $\nu_{RF}\tau$ increments of 0.08 cycles. The gray scale contours in each plot range from ≥90% (black) through ≤50% (white) of the maximum coherence intensity; dashed lines represent the $\theta_2/\theta_1 = 2$ condition.

verified with ^{23}Na MQMAS NMR experiments on polycrystalline Na_2SO_4 and $Na_2C_2O_4$ samples. Figure 2 illustrates representative results arising from these $S = \frac{3}{2}$ measurements. It compares the MQ generation performance of single- and composite-pulse approaches, as detected in MQMAS acquisitions involving a fixed MQ evolution time (equal to one rotor period) and a final conversion pulse of 0.2 cycles. The main features of the numerical calculations are reproduced by these experimental results, including a maximum in the MQ coherence excitation corresponding to composite pulses with $\tau_2/\tau_1 \approx 2$ and these signals exceeding their single pulse counterparts by a ratio of about 1.3.

These results corroborate again the validity of using a simplified Hamiltonian like that introduced in Eq. [3] when trying to model relevant experimental situations. An interesting feature of this Hamiltonian is that despite being represented by a 4×4 matrix it is susceptible to analytical diagonalization (*40, 46*), thus enabling an explicit propagation of the spin density matrix throughout the course of the experiment. This characteristic can be exploited in order to better understand the physical origins of the composite pulse's superior MQ excitation per-

formance. We decided to undertake this calculation by focusing on the effects that an arbitrary $(\tau_1)_x(\tau_2)_\phi$ sequence will have on the evolution of the matrix elements, and then simplifying the resulting expressions by expanding the eigenvalues and eigenvectors of $H(t)$ in powers of $\nu_{RF}/[e^2qQ/h]$ (*38, 40*). The leading terms in these expansions lead to

$$\frac{\partial|\rho_{14}|^2}{\partial\phi} = 9a^2\cdot\left\{6\sin 3\phi\sin\nu_{13}\tau_1\sin\nu_{13}\tau_2\cdot\begin{bmatrix}\cos 3\phi\cdot(\sin\nu_{13}\tau_1+2\cos\nu_{13}\tau_1)\cdot\sin\nu_{13}\tau_2\\ -\cos\nu_{13}\tau_1\cos\nu_{13}\tau_2\end{bmatrix}\right\} \quad [10a]$$

$$\frac{\partial|\rho_{14}|^2}{\partial\tau_1} = 9a^2\nu_{13}\begin{bmatrix}\sin 2\nu_{13}\tau_1\cdot(\cos^2\nu_{13}\tau_2-\sin^2\nu_{13}\tau_2\cos^2 3\phi)\\ +\cos 2\nu_{13}\tau_1\cdot(\sin 2\nu_{13}\tau_2\cos 3\phi+\sin^2\nu_{13}\tau_2\sin^2 3\phi)\end{bmatrix} \quad [10b]$$

$$\frac{\partial|\rho_{14}|^2}{\partial\tau_2} = 9a^2\nu_{13}\left\{\begin{matrix}[\cos 2\nu_{13}\tau_1+\sin^2 3\phi\cdot(\sin 2\nu_{13}\tau_1+\sin^2\nu_{13}\tau_1)]\cdot\sin 2\nu_{13}\tau_2\\ +\sin 2\nu_{13}\tau_1\cos 2\nu_{13}\tau_2\cos 3\phi\end{matrix}\right\}. \quad [10c]$$

$$\begin{aligned}&\rho_{14}(\tau_1,\tau_2,\phi)\\ &\quad=[\rho_{41}(\tau_1,\tau_2,\phi)]^*\\ &\quad=3ai\begin{bmatrix}\exp(-3i\phi)\cdot\cos\nu_{13}\tau_1\sin\nu_{13}\tau_2\\ -\sin\nu_{13}\tau_1\cdot(i\sin 3\phi\sin\nu_{13}\tau_2-\cos\nu_{13}\tau_2)\end{bmatrix},\end{aligned} \quad [6]$$

where

$$\nu_{13} = \frac{3}{8}\left[\frac{\nu_{rf}}{\nu_q(\theta,\varphi)}\right]^2\nu_{rf} \quad [7]$$

describes the orientation-dependent nutation frequency introduced by the RF pulses, a is again the Boltzmann factor, and $i=\sqrt{-1}$. It can be easily verified that for $\phi=0$ Eq. [6] reduces to

$$\rho_{14}(\tau_1,\tau_2,\phi=0) = 3ai\sin[\nu_{13}(\tau_1+\tau_2)], \quad [8]$$

thus blurring the distinction between τ_1 and τ_2 and leading to sinusoidal single-crystal oscillations of amplitude $3a$ similar to those we have described in an earlier report (*22*). On the other hand on reverting to the use of a single pulse, Eq. [6] predicts

$$\begin{aligned}&\rho_{14}(\tau_1,\tau_2,\phi)\\ &\qquad=\begin{cases}3ai\sin(\nu_{13}\tau_1), & \text{if } \tau_2=0\\ 3ai\exp(-3i\phi)\sin(\nu_{13}\tau_2), & \text{if } \tau_1=0\end{cases}\end{aligned} \quad [9]$$

in accordance with the well-known behavior or MQ coherence excitations (*38–40*).

It is possible to exploit the analytical form of Eq. [6] in order to derive the conditions that will maximize the MQ excitation for arbitrary single-crystal orientations, and then compute the values that the spin coherences will then adopt. Since the ρ_{14} elements are complex, searching for a maximum MQMAS signal entails finding the parameters that will simultaneously satisfy the $\nabla|\rho_{14}|^2=0$ conditions given by

The first of these gradients can be nulled for arbitrary ν_{13} values by either

$$\nu_{13}\tau_1 = k\pi, \quad k=0,1,2,\cdots \quad [11a]$$

$$\nu_{13}\tau_2 = l\pi, \quad l=0,1,2,\cdots \quad [11b]$$

$$3\phi = m\pi, \quad m=0,1,2,\ldots, \quad [11c]$$

or by selecting

$$tg\nu_{13}\tau_2 = \frac{1}{\cos 3\phi\cdot(tg\nu_{13}\tau_1+2)} \quad [12]$$

which will null the right-hand bracketed term in Eq. [10a]. Equations [11] include the single-pulse nutation cases (τ_1, $\tau_2=0$), and can thus be considered as generalizations of the behavior described in Eqs. [8] and [9]. Indeed these conditions lead to maximum $|\rho_{14}|$ values of $3a$, which do not correspond to the absolute signal maximum. To find the latter Eq. [12] needs to be chosen and then replaced into Eqs. [10b], [10c], which yield the revised conditions

$$tg2\nu_{13}\tau_1 = \frac{\sin 2\nu_{13}\tau_2\cos 3\phi+\sin^2\nu_{13}\tau_2\sin^2 3\phi}{\sin^2\nu_{13}\tau_2\cos^2 3\phi-\cos^2\nu_{13}\tau_2} \quad [13a]$$

$$\begin{aligned}&tg2\nu_{13}\tau_2\\ &\quad=-\frac{\cos 3\phi}{ctg2\nu_{13}\tau_1+\sin^2 3\phi\cdot\left(\frac{1}{2}tg\nu_{13}\tau_1+1\right)}.\end{aligned} \quad [13b]$$

The simultaneous solution of these equations can again be

achieved by a number of different $(\nu_{13}\tau_1, \nu_{13}\tau_2, \phi)$ combinations. Within a $[0, \pi]$ interval these include

$$\nu_{13}\tau_1 = 3\pi/4,\ \nu_{13}\tau_2 = \pi/2,$$
$$\phi = (2n + 1)\pi/6\ (n = 0, 1, 2), \qquad [14]$$

which if replaced into Eq. [6] will lead to $|\rho_{14}| = 0$ and thus represent a signal minimum, and

$$\nu_{13}\tau_1 = \pi/4,\ \nu_{13}\tau_2 = \pi/2,$$
$$\phi = (2n + 1)\pi/6\ (n = 0, 1, 2), \qquad [15]$$

which after substitution in Eq. [6] result in the absolute MQ excitation maximum $|\rho_{14}| = 3\sqrt{2}a$. The correctness of these algebraic derivations can be independently verified by graphical means with a three-dimensional plot of $|\rho_{14}|$ over the $0 \leq \nu_{13}\tau_1, \nu_{13}\tau_2, \phi \leq \pi$ interval (Fig. 3), which confirms the behavior predicted by Eqs. [11]–[15]. The summary of this single-crystal analysis is that composite pulses with $\tau_2/\tau_1 = 2$ and $\phi = \pi/2$ will provide an optimum ρ_{14} excitation,whose signals will exceed by $\sqrt{2}$ the maximum available from conventional single-pulse nutations. Although these numbers can be expected to change somewhat as calculations are extended to powders, these analytical predictions constitute with all likelihood the basis for the ''brute force'' numerical parameters arising from the plots depicted in Fig. 1.

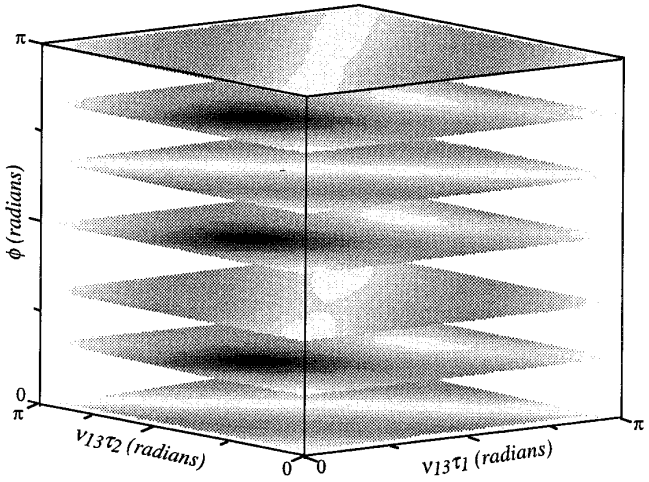

FIG. 3. Dependence of the triple-quantum coherence magnitude excited by a $(\tau_1)_x(\tau_2)_\phi$ on a spin-$\frac{3}{2}$ single-crystallite ($|\rho_{14}|$, Eq. [6]), as a function of the experimental variables τ_1, τ_2, ϕ. The gray scale ranges from ≥90% (black) to ≤40% (white) of the maximum intensity, and shows the appearance of absolute maxima at $\nu_{13}\tau_1 = \pi/4$, $\nu_{13}\tau_2 = \pi/2$, $\phi = \pi/6$, $\pi/2$, $5\pi/6$ radians.

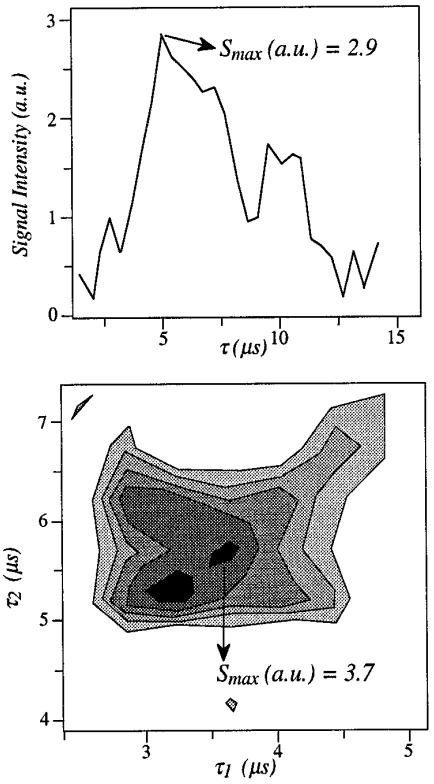

FIG. 2. Experimental ^{23}Na triple-quantum excitation profiles obtained from a $Na_2C_2O_4$ powder using single- (top) and composite-pulse (bottom) RF nutation sequences. Data were acquired in both cases under identical on-resonance conditions using MAS ($\nu_r \approx 6$ kHz), 256 scans/point, $\nu_{RF} = 150$ kHz. Contours in the 2D plot are equally spaced between 50 and 90% of the maximum signal intensity.

Shielding Offset Effects

As has been the case with the majority of MQMAS NMR analyses that have hitherto been reported, the preceding paragraph focused on the generation of coherences without explicitly considering potential complications arising from chemical shift effects. Although this is a safe approximation when dealing with alkali metals or light main group elements possessing relatively small shielding scales ($\leq 0.1 \cdot \nu_{RF}$), shift effects may become potentially important complications toward the excitation of MQ coherences in other cases. This is quantitatively illustrated by the numerical excitation profiles presented in Fig. 4, which show how isotropic and anisotropic shielding effects can decrease the maximum amount of coherence achievable from single-pulse RF nutations even when considerably smaller than the RF excitation field. In addition to an overall decrease in intensity isotropic shifts also introduce noticeable oscillations in the time-domain profiles of the MQ nutation, which apparently interfere with one another in the anisotropic case.

In some extreme situations, the excitation complications brought about by shielding effects may prevent the acquisition of MQMAS data altogether even when dealing with sites possessing small quadrupole couplings. A case in point is presented in Fig. 5, which compares MAS and MQMAS

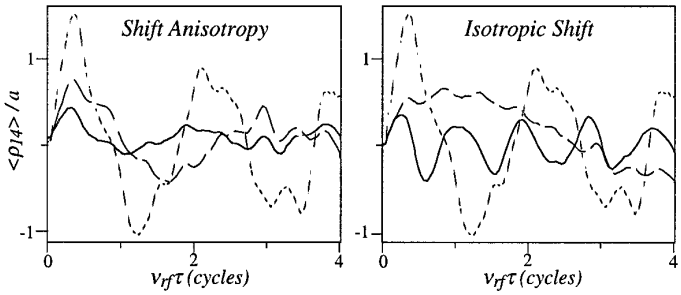

FIG. 4. Time dependences of $S = \frac{3}{2}$ triple-quantum excitation profiles in the presence of isotropic and anisotropic chemical shifts under the effects of a single-pulse excitation sequence. Plots were calculated assuming $e^2qQ/h = 2.6$ MHz, $\eta = 0$, $\nu_{RF} = 100$ kHz, and the following ratios between the strengths of the shielding and RF interactions: 0 (---), 0.2 (– –), 0.4 (—).

cobalt NMR spectra (^{59}Co, $S = \frac{7}{2}$) for the model compound $K_3[Co(CN)_6]$ and for a synthetic [Co(tetraphenylporphyrin-bismethylimidazole)]BF_4 complex. Even though the cobalt site in the former compound has a larger quadrupole coupling constant than in the latter (5.9 vs 3.5 MHz) (*44*, *47*), the porphyrin complex yields little MQMAS data even after extensive signal averaging due to its much larger shielding anisotropy. Calculations predict that similar effects can be expected in the presence of large second-order quadrupole anisotropies, a behavior which we have experimentally verified in 4.7-T ^{35}Cl MQMAS NMR investigations (data not shown).

In view of the severe detrimental effects that shielding offsets can have on the single-pulse excitation of MQ coherences, we decided to explore the potential advantages that may result from employing two-pulse excitation sequences of the type depicted in Eq. [1]. A full numerical search similar to that described in the preceding paragraph but incorporating shielding offsets was thus carried out, and it revealed that a $\Delta = 0$ composite pulse is again a superior way of exciting MQ coherences provided that an $x-\bar{x}$ scheme (rather than an $x-y$ one) is employed as offsets exceed values of approximately $\nu_{RF}/10$. Even under these optimal conditions the overall excitation of MQ coherences becomes less efficient in the presence of substantial chemical shifts, as may be appreciated from the calculated and experimental offset dependences presented in Fig. 6. Furthermore, by contrast to the simple $\tau_2/\tau_1 \approx 2$ optimization recipe that could be derived in the absence of offsets, the optimized durations

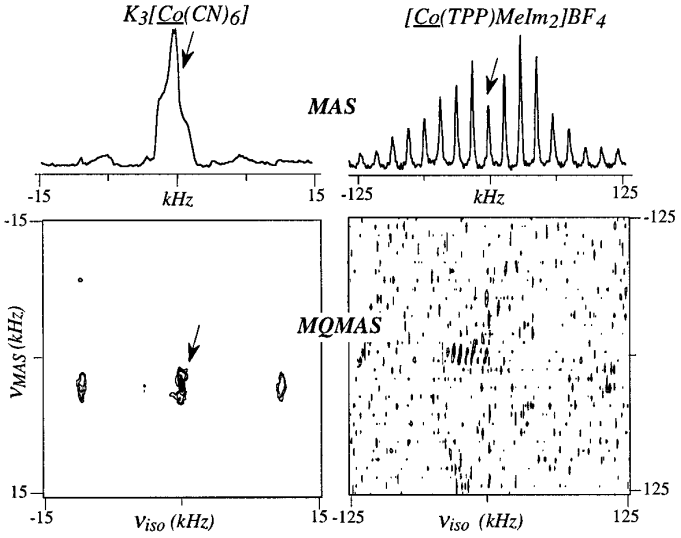

FIG. 5. Comparison between MAS and sheared MQMAS ^{59}Co NMR results observed for two different single-site cobalt complexes ($B_0 = 4.7$ T, $\nu_r \approx 10$ kHz). Acquisition of the hexacyano data involved 256 scans for the MAS trace and 1200 scans/t_1 increment (128 t_1 values) for the MQMAS. The porphyrin MAS spectrum was collected using 2000 scans while its MQMAS required 67000 scans/t_1 increment (4 days continuous acquisition). Notice the much poorer S/N of this spectrum, consequence of the about 3000-ppm shift anisotropy characterizing its cobalt site. Arrows indicate the positions of the spinning centerbands.

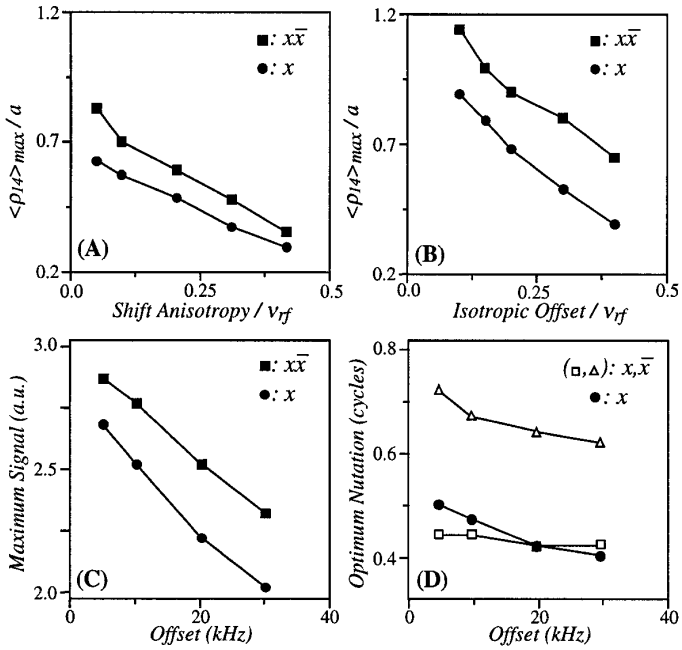

FIG. 6. (A, B) Theoretical dependences predicted for the maximum MQ coherence excitation resulting upon employing single- (●) and $x-\bar{x}$ composite- (■) pulse sequences, as a function of the relative strength of the shielding interaction. Calculations are the result of multidimensional τ_1, τ_2 powder searches carried out for individual shielding values under the assumptions $\nu_{RF} = 100$ kHz, $e^2qQ/h = 2.6$ MHz, $\eta = 0$. (C) ^{23}Na NMR corroboration of the theoretical predictions, evidenced by the largest $Na_2C_2O_4$ MQMAS signals observed from single- and composite-pulse experiments as a function of the transmitter offset. (D) RF nutation angles leading to the maximum excitation signals plotted in (C) for the single- (●) and composite-pulse (□ = θ_x, △ = $\theta_{\bar{x}}$) experiments. Notice that in agreement with the predictions of Fig. 4, the optimized single-pulse nutation angles shorten slightly with increasing offsets.

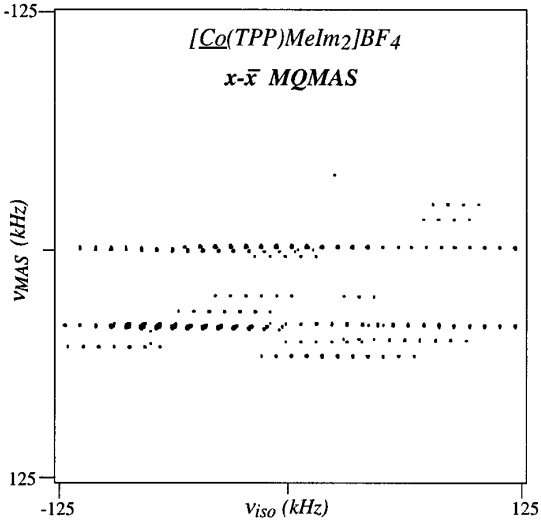

FIG. 7. ^{59}Co MQMAS NMR spectrum obtained from the cobaltoporphyrin complex examined in Fig. 4 using an $x-\bar{x}$ composite pulse excitation sequence. The excitation pulse lengths (τ_x = 4 μs, $\tau_{\bar{x}}$ = 5.5 μs) were optimized on the basis of *a priori* knowledge of ν_{RF} and of the site's shielding and quadrupole couplings; all other acquisition parameters are as described in the legend to Fig. 5.

that are now predicted for the x and $\bar{x}$ nutations angles are dependent on the particular combination of e^2qQ/h, chemical shift, and ν_{RF} values involved. Due to this reason the use of composite pulses for exciting MQ coherences in the presence of strong shielding effects is, at least in its present stage, a useful alternative only if accompanied by suitable *a priori* calculations of the pulse angles by computational means. These calculations require in turn an approximate knowledge of the quadrupole and shielding couplings involved. When this kind of information is available the optimized composite pulse excitation may lead to substantial gains in spectral S/N; for the cobaltoporphyrin complex mentioned above an improvement of almost 100% could be achieved in this manner, allowing its MQMAS signal to clearly emerge from out of the background noise (Fig. 7).

DISCUSSION AND CONCLUSIONS

The results introduced in the previous section evidence the advantages that may result from using composite pulse schemes in MQMAS NMR. In the absence of strong offset effects sizable gains in S/N could be demonstrated both numerically and experimentally by employing relatively general and simple $x-y$ excitation conditions. Although our discussion centered exclusively around spin-$\frac{3}{2}$ powders, gains were also observed upon extending these calculations to higher spin numbers. Composite pulse excitations were also found superior to conventional nutations in the presence of large chemical shifts, but the optimization of these experiments ended up being sensitive to the site's coupling parameters and thus likely to be useful only in combination with preliminary numerical calculations. *In lieu* of these optimized pulse sequence the only strategies currently available for bypassing the chemical shift complications involve increasing the RF field strength or operating at smaller Larmor frequencies, two approaches which suffer from evident limitations.

In addition to its practical advantages, the signal enhancement brought about by $x-y$ composite pulses opens up interesting questions related to the maximum ''amounts'' of MQ coherences that can actually be expected from quadrupolar spins. For the case of a spin-$\frac{3}{2}$ single crystal and in analogy with the nutation of an isolated spin-$\frac{1}{2}$, one could have assumed that the complete transfer of the *3a* triple-quantum populations into ρ_{14} triple-quantum elements (Eq. [8]) would define the upper limit of the excitation. This expectation is exceeded by a $\sqrt{2}$ factor in the composite pulse excitation owing to the latter's ability to extract triple-quantum coherences from *all* the Zeeman populations in the spin manifold. In fact, a principal value analysis on the upper entropic limit (*48*) for the MQ excitation process reveals that for $S = \frac{3}{2}$ the maximum which can be expected upon starting from thermal equilibrium is $\rho_{14} = 2\sqrt{5}a$. Given the $\rho_{14} = 3\sqrt{2}a$ value reached under the conditions in Eq. [15], it follows that at most a 5% efficiency increase can be expected from further manipulations. Indeed we have attempted to introduce additional improvements on the $x-y$ excitation sequence by considering the use of additional pulses, but numerical simulations revealed that only marginal gains on the order of 1% occur upon implementing these more complex procedures.

In addition to these excitation investigations we have employed numerical means to explore the potential of two-pulse schemes like that presented in Eq. [1] for providing an improved conversion of the MQ coherences to the single-quantum observables. The results of these calculations, however, are not described here in any detail, since they failed to reveal significant advantages with respect to their single-pulse counterparts. The relative enhancements that we observed for the conversion process on spin-$\frac{3}{2}$ powders amounted in all cases to less than 10%. Alternative approaches will thus be needed for optimizing the efficiency of this final conversion step, which is in fact responsible for much of the signal losses occurring in MQMAS experiments.

ACKNOWLEDGMENTS

We are grateful to Dr. Veronica Frydman (UIC) for the preparation of the cobaltoporphyrin chelate, and to one of the paper's Reviewers for his/her insightful comments. This work was supported by the National Science Foundation through Grants DMR-9420458 and CHE-9502644 (CAREER Award). A.M. and L.M. acknowledge UIC for Fellowships; L.F. is a Beckman Young Investigator (1996-1998), Camille Dreyfus Teacher-Scholar (1996-2001), University of Illinois Junior Scholar (1997-2000), and Alfred P. Sloan Fellow (1997-2000).

REFERENCES

1. C. A. Fyfe, ''Solid State NMR for Chemists,'' CFC Press, Ontario (1983).
2. K. Schmidt-Rohr and H. W. Spiess, ''Multidimensional Solid-State NMR and Polymers,'' Academic Press, London (1994).
3. E. R. Andrew, A. Bradbury, and R. G. Eades, *Nature* **182,** 1659 (1958).
4. I. J. Lowe, *Phys. Rev. Lett.* **2,** 285 (1959).
5. J. S. Waugh, L. M. Huber, and U. Haeberlen, *Phys. Rev. Lett.* **20,** 180 (1968).
6. A. Abragam, ''The Principles of Nuclear Magnetism,'' Oxford University Press, Oxford (1985).
7. C. P. Slichter, ''Principles of Nuclear Magnetic Resonance,'' Springer-Verlag, New York (1990).
8. M. H. Cohen and F. Reif, *Solid State Phys.* **5,** 321 (1957).
9. A. H. Silver and P. J. Bray, *J. Chem. Phys.* **29,** 984 (1958).
10. E. Kundla, A. Samoson, and E. Lippmaa, *Chem. Phys. Lett.* **83,** 229 (1981).
11. S. Ganapathy, S. Schramm, and E. Oldfield, *J. Chem. Phys.* **77,** 4360 (1982).
12. A. Llor and J. Virlet, *Chem. Phys. Lett.* **152,** 248 (1988).
13. E. W. Wooten, K. T. Muller, and A. Pines, *Acc. Chem. Res.* **25,** 209 (1992).
14. A. Samoson, E. Lippmaa, and A. Pines, *Mol. Phys.* **65,** 1013 (1988).
15. K. T. Mueller, B. Q. Sun, G. C. Chingas, J. W. Zwanziger, T. Terao, and A. Pines, *J. Magn. Reson.* **86,** 470 (1990).
16. L. Frydman and J. S. Harwood, *J. Am. Chem. Soc.* **117,** 5367 (1995).
17. J. V. Hanna, M. E. Smith, and H. J. Whitfield, *J. Am. Chem. Soc.* **118,** 5772 (1996).
18. H. Kraus, R. Prins, and A. P. N. Kentgents, *J. Phys. Chem.* **100,** 16336 (1996).
19. D. Massiot, B. Tonzo, D. Trumean, J. P. Coutures, J. Virlet, P. Florian, and P. J. Grandinetti, *Solid State NMR* **6,** 73 (1996).
20. J. H. Baltisberger, Z. Xu, J. F. Stebbins, S. H. Wang, and A. Pines, *J. Am. Chem. Soc.* **118,** 7209 (1996).
21. S.-J. Hwang, C. Fernandez, J. P. Amoureux, J. Cho, S. W. Martin, and M. Pruski, *Solid State NMR* **8,** 109 (1997).
22. A. Medek, J. S. Harwood, and L. Frydman, *J. Am. Chem. Soc.* **117,** 12779 (1995).
23. C. Fernandez and J. P. Amoureux, *Chem. Phys. Lett.* **242,** 449 (1995).
24. G. Wu, D. Rovnyak, and R. G. Griffin, *J. Am. Chem. Soc.* **118,** 9326 (1996).
25. G. Wu, D. Rovnyak, B. Sun, and R. G. Griffin, *Chem. Phys. Lett.* **249,** 210 (1996).
26. J. P. Amoureux, C. Fernandez, and L. Frydman, *Chem. Phys. Lett.* **259,** 347 (1996).
27. D. Massiot, *J. Magn. Reson. A* **122,** 240 (1996).
28. D. Massiot, B. Tonzo, D. Trumean, J. P. Coutures, J. Virlet, P. Florian, and P. J. Grandinetti, *Solid State NMR* **6,** 73 (1996).
29. S. P. Brown, S. J. Heyes, and S. Wimperis, *J. Magn. Reson. A* **119,** 280 (1996).
30. A. Samoson, *J. Magn. Reson. A* **121,** 209 (1996).
31. J. P. Amoureux, C. Fernandez, and S. Steuemagel, *J. Magn. Reson. A* **123,** 116 (1996).
32. S. P. Brown and S. Wimperis, *J. Magn. Reson.* **124,** 279 (1997).
33. M. J. Duer and C. Stourton, *J. Magn. Reson.* **124,** 189 (1997).
34. S. H. Wang, Z. Xu, J. H. Baltisberger, L. M. Bull, J. F. Stebbins, and A. Pines, *Solid State NMR* **8,** 1 (1997).
35. S. Ding and C. A. McDowell, *Chem. Phys. Lett.* **270,** 81 (1997).
36. G. Drobny, A. Pines, S. Sinton, D. P. Weitekamp, and D. Wemmer, *Faraday Disc. Chem. Soc.* **13,** 49 (1979).
37. G. Bodenhausen, *Prog. NMR Spectrosc.* **14,** 137 (1981).
38. A. Wokaun and R. R. Ernst, *J. Chem. Phys.* **67,** 1752 (1977).
39. S. Vega and A. Pines, *J. Chem. Phys.* **66,** 5624 (1977).
40. S. Vega, *J. Chem. Phys.* **68,** 5518 (1978).
41. S. Vega and Y. J. Naor, *J. Chem. Phys.* **75,** 75 (1981).
42. N. C. Nielsen, H. Bildsøe, and H. J. Jakobsen, *Chem. Phys. Lett.* **191,** 205 (1992).
43. M. H. Levitt, *Prog. NMR Spectrosc.* **18,** 61 (1986).
44. A. Medek, V. Frydman, and L. Frydman, *J. Phys. Chem. B* **101,** 8959 (1997).
45. L. Marinelli and L. Frydman, *Chem. Phys. Lett.* **275,** 188 (1997).
46. R. Jannsen and W. S. Veeman, *J. Chem. Soc., Faraday Trans.* **84,** 3747 (1988).
47. J. A. Lourens and E. C. Reynhardt, *Phys. Stat. Sol. (a)* **11,** 739 (1972).
48. O. W. Sorensen, *Prog. NMR Spectrosc.* **21,** 503 (1989).